

Cite this: *Nanoscale Adv.*, 2024, 6,
2945Received 6th March 2024
Accepted 11th April 2024

DOI: 10.1039/d4na00198b

rsc.li/nanoscale-advances

Single-particle Förster resonance energy transfer from upconversion nanoparticles to organic dyes†

Jialing Hu, Fei Zhao, Huan Ling, Yunxiang Zhang and Qian Liu *

Single-particle detection and sensing, powered by Förster resonance energy transfer (FRET), offers precise monitoring of molecular interactions and environmental stimuli at a nanometric resolution. Despite its potential, the widespread use of FRET has been curtailed by the rapid photobleaching of traditional fluorophores. This study presents a robust single-particle FRET platform utilizing upconversion nanoparticles (UCNPs), which stand out for their remarkable photostability, making them superior to conventional organic donors for energy transfer-based assays. Our comprehensive research demonstrates the influence of UCNPs' size, architecture, and dye selection on the efficiency of FRET. We discovered that small particles (~14 nm) with a Yb³⁺-enriched outermost shell exhibit a significant boost in FRET efficiency, a benefit not observed in larger particles (~25 nm). 25 nm UCNPs with an inert NaLuF₄ shell demonstrated a comparable level of emission enhancement via FRET as those with a Yb³⁺-enriched outermost shell. At the single-particle level, these FRET-enhanced UCNPs manifested an upconversion green emission intensity that was 8.3 times greater than that of their unmodified counterparts, while maintaining notable luminescence stability. Our upconversion FRET system opens up new possibilities for developing more effective high-brightness, high-sensitivity single-particle detection, and sensing modalities.

1 Introduction

Single-particle detection and sensing is at the forefront of single-molecule imaging, enabling us to observe and analyze individual particles down to the nanometer scale.^{1–7} This capability has been transformative in dissecting complex biological systems and detecting trace amounts of substances with exceptional specificity and sensitivity. The fundamental principle of this technique hinges on tracking distinct optical properties such as fluorescence^{8,9} and plasmon resonance^{10–12} of individual nanoparticles or molecules. Förster resonance energy transfer (FRET) is a pivotal technique often employed for sensitive single-particle detection.^{13–16} FRET's ability to detect minute distance changes between a donor and an acceptor molecule renders it invaluable for real-time monitoring of molecular interactions and conformational shifts.¹⁷ Yet, the conventional fluorophores employed in FRET are prone to rapid photobleaching, which diminishes their fluorescence upon light exposure, thus constraining their effectiveness over prolonged or intensive imaging sequences.¹⁸ Within this framework, upconversion nanoparticles (UCNPs) have surfaced as a pivotal innovation. Their resistance to photobleaching

presents a durable alternative for extended imaging applications, representing a significant leap forward in the domain of single-particle detection.^{19–22}

UCNPs are typically synthesized by doping lanthanide ions, such as Yb³⁺, Er³⁺, or Tm³⁺, into a host material. These UCNPs are renowned for their distinctive anti-Stokes luminescence, a process where the absorption of multiple near-infrared (NIR) photons results in the emission of photons at shorter wavelengths through a complex energy transfer sequence.^{23–30} The NIR excitation characteristics of UCNPs are especially beneficial as they minimize autofluorescence, thus facilitating background-free detection. Additionally, the lanthanide ions' 4f electrons are effectively shielded, bestowing UCNPs with sharp emission peaks and exceptional optical stability. These advantages render UCNPs an ideal FRET donor for various biological applications, such as bioimaging,^{31–33} optical sensing^{34–36} and multimodal theranostics.^{37–40}

Organic dyes are commonly used as FRET acceptors to harvest energy from UCNPs. Due to the inherently forbidden radiative transitions of lanthanide ions within UCNPs, these emissions are characterized by prolonged lifetimes and diminished radiative rates, often resulting in significant non-radiative energy losses within UCNPs' complex energy transfer networks. Therefore, organic dyes with fast radiation rates were selected as FRET acceptors to enhance the upconversion emission.^{41–43} Different from the previously reported dye-sensitization, which utilizes the energy transfer process from

Department of Chemistry and Shanghai Key Laboratory of Molecular Catalysis and Innovative Materials, Fudan University, Shanghai 200438, China. E-mail: qianliu@fudan.edu.cn

† Electronic supplementary information (ESI) available. See DOI: <https://doi.org/10.1039/d4na00198b>



dye to UCNPs, this enhancement strategy, termed “FRET-enhanced upconversion” in this manuscript, involves transferring energy from UCNPs to fluorescent dyes. Moreover, the excitation laser used to energize lanthanide ions, typically at 980 nm or 808 nm, does not excite organic dyes, conferring the UCNPs-organic dye FRET pairs with enhanced resistance to photobleaching.

In this study, we showcased single-particle FRET from UCNPs to organic dyes, achieved through systematic optimization of the UCNPs size and structural configuration, alongside the selection of appropriate dye species. By conducting experiments in a hydrophilic environment, we successfully realized an 8.3-fold enhancement by using the FRET-enhanced green upconversion emission at the single-particle level.

2 Results and discussion

In the composition of UCNPs, Yb^{3+} commonly served as a sensitizer, capturing excitation light energy and facilitating its transfer to the emitter of Er^{3+} . With organic acceptors decorated on the UCNPs surface, the excited-state energy of Er^{3+} can be further transferred to these surface-anchored acceptors through the FRET process. Given the strong distance dependence of FRET, the core-only YbEr or core-shell Yb@YbEr architecture with a shorter donor-acceptor (D-A) distance was typically favored.⁴⁴ However, to enhance the upconversion luminescence, an outermost protective shell of appropriate thickness may be essential to mitigate the severe surface quenching, despite the reduced FRET efficiency due to the longer D-A distance induced by the shell. An inherent trade-off between reducing surface quenching and promoting short-range energy transfer processes must be considered.

Our previous studies have shown that an Yb^{3+} -doped outermost shell outperforms an inert shell, especially at high-power densities at the single-particle level, due to its enhanced photon capture capabilities.⁴⁵ Building on this finding, we hypothesized that in a FRET-enhanced upconversion system, an Yb^{3+} -enriched outermost shell could capture more photons and transfer them to the inner FRET donor Er^{3+} through energy migration, thus enhancing the FRET process compared to the inert-shelled UCNPs (Fig. 1a and b). The core-shell (CS) UCNPs consisting of $\text{NaYb}_{0.92}\text{Er}_{0.08}\text{F}_4@/\text{NaLu}_{1-x}\text{Yb}_x\text{F}_4$ were synthesized *via* the solvothermal method according to previous work with slight modifications to acquire the appropriate size and doping concentrations.⁴⁶ The core was designed with a molar doping ratio of 92% Yb to 8% Er for the sensitizer and activator ions, respectively, aiming for bright single-particle emission.⁴⁶ Transmission electron microscopy (TEM) images confirmed the uniform size of the synthesized core UCNPs with a diameter of 10.8 ± 0.9 nm (Fig. 1c). A $\text{NaLu}_{1-x}\text{Yb}_x\text{F}_4$ ($x = 0, 0.25, 0.5, 0.75, 1$) shell with a thickness of approximately 2 nm was subsequently deposited on this core, enabling the systematic variation of the Yb^{3+} doping concentration. All of these core-shell particles had a uniform size of ~ 14 nm and exhibited good dispersibility (Fig. 1d-h), and were named $\text{CS}^{14}\text{-NaLu}_{1-x}\text{Yb}_x\text{F}_4$. X-ray powder diffraction (XRD) demonstrated the hexagonal phase of these UCNPs (Fig. S1†). Fig. S2† shows the upconversion spectra of

these UCNPs. The inert-shelled UCNPs of $\text{CS}^{14}\text{-NaLuF}_4$ were obviously brighter than the active-shelled UCNPs, and the upconversion intensity gradually decreased with the increase in Yb^{3+} doping concentration in the shell. This result is consistent with previous research where higher Yb^{3+} doping leads to severe non-radiative surface quenching.⁴⁵

We selected the commercial cyanine dye sulfo-Cy3 as the FRET acceptor, which exhibited a strong absorption band with a peak at 559 nm and substantial spectral overlap with the green emission at 541 nm of Er^{3+} in UCNPs, facilitating the sufficient FRET energy transfer from UCNPs to dyes. Sulfo-Cy3 could coordinate to the surface Ln^{3+} ions of UCNPs *via* its sulfonate groups, enabling a close energy transfer distance, which is critical in the FRET process.⁴³ We adopted the direct ligand-exchange method to decorate the UCNPs with dyes.⁴⁷ As shown in Fig. S3,† these sulfo-Cy3 decorated UCNPs (denoted as sulfo-Cy3-CS-NaLu_{1-x}Yb_xF₄) dispersed well without apparent aggregation. After the addition of sulfo-Cy3, all of these sulfo-Cy3-UCNPs showed evident FRET-enhanced upconversion (Fig. S2 and S4†), indicating feasible FRET energy transfer from UCNPs to sulfo-Cy3. However, as shown in Fig. 1i, the emission enhancement depended on the doping concentration of Yb^{3+} in the shell. The UCNPs with 75% Yb^{3+} and 100% Yb^{3+} doping displayed the highest relative brightness enhancement of 6-fold with the addition of sulfo-Cy3 (Fig. 1i and j). Besides, the response of UCNPs decay kinetics was diminished with the decrease in Yb^{3+} doping concentration (Fig. S5†). These results could be explained by that sulfo-Cy3 here provided a new fast radiative pathway, in which more excited Yb^{3+} tended to transfer energy to Er^{3+} and subsequently to the dye molecules on the surface by FRET, mitigating the nonradiative quenching effect in the active-shelled UCNPs. The increased non-radiative quenching led by higher Yb^{3+} doping in the shell could be alleviated by sulfo-Cy3, resulting in a greater emission enhancement factor (Fig. S6†).

Although heavily doped Yb^{3+} ions in the UCNPs structure are crucial for efficient upconversion luminescence, the Yb^{3+} network may accumulate and transfer excited state energy, and repopulate the excited FRET donor Er^{3+} ions as soon as they donate energy to the acceptor dye molecules and return to their ground states. As a consequence, the excess Yb^{3+} ions may alter the luminescence kinetic decay response of the FRET system and impair the reliability of luminescence decay as a FRET indicator.⁴⁴ Therefore, we primarily evaluated the FRET efficiency through intuitive upconversion enhancement, while utilizing the luminescence decay kinetics of Er^{3+} ions to explain the underlying mechanism.

To further increase the FRET-enhanced upconversion, we explored the influence of the dye structure on upconversion enhancement. In addition to the sulfo-Cy3 used above, we also selected two other dyes, sulfo-Cy3-amine and sulfo-rhodamine B; their maximum absorptions were located at 564 and 554 nm, respectively, satisfying the requirement for spectral overlap (Fig. S7†). Compared with UCNPs alone, sulfo-rhodamine B-enhanced and sulfo-Cy3-enhanced upconversion produced significant enhancement of 7.1 and 4.5 times at their optimal concentration, respectively (Fig. S8 and S9†). However,



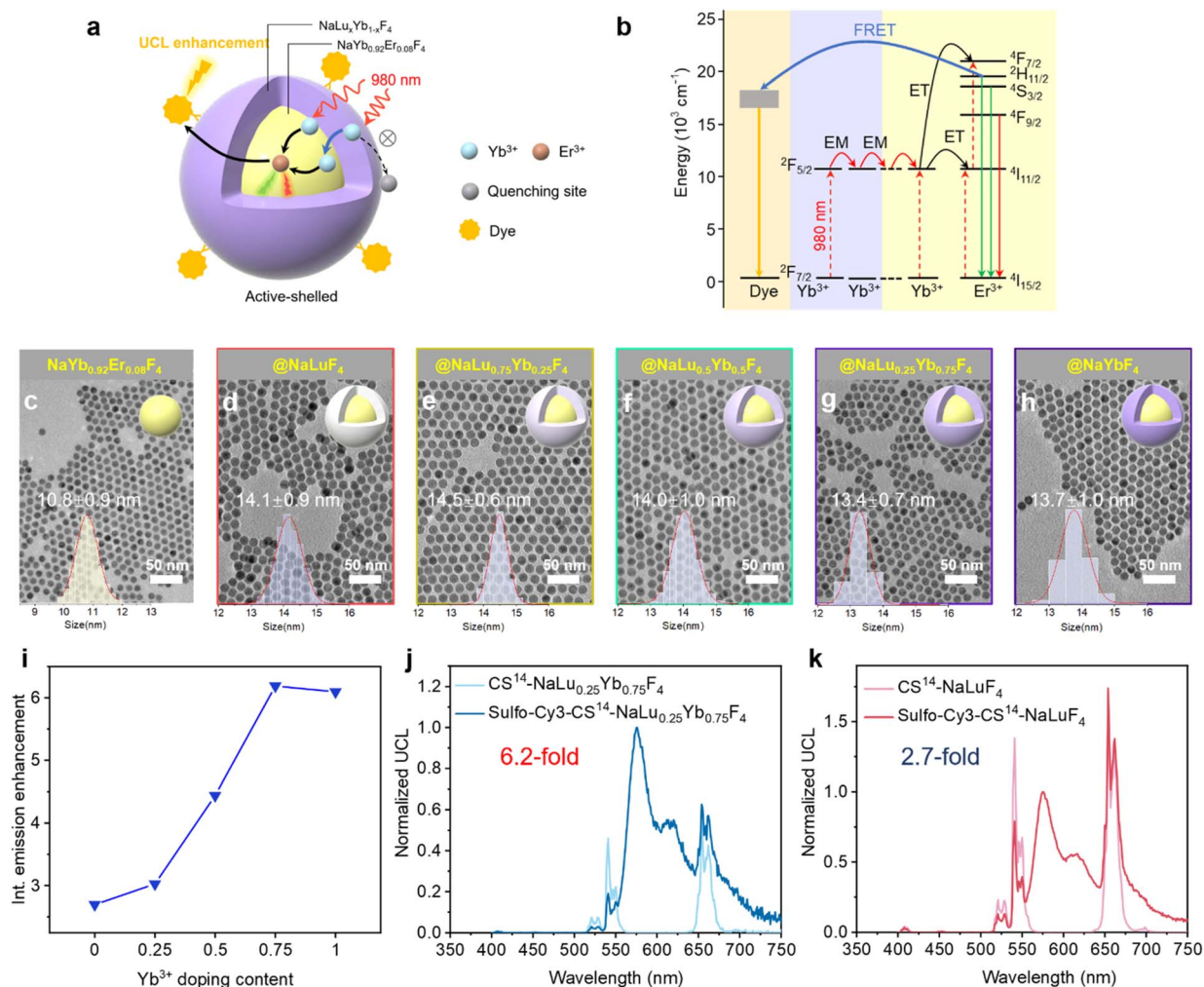


Fig. 1 FRET-enhanced upconversion of core-shell UCNP with 980 nm irradiation. (a) Schematic of active-shelled core-shell UCNP ($\text{NaYb}_{0.92}\text{Er}_{0.08}\text{F}_4@ \text{NaLu}_{1-x}\text{Yb}_x\text{F}_4$) emission enhancement through FRET to a dye. (b) The Jablonski diagram of the corresponding FRET-enhanced upconversion mechanism. ET: energy transfer; EM: energy migration. (c–h) TEM images and size distributions of the as-prepared core $\text{NaYb}_{0.92}\text{Er}_{0.08}\text{F}_4$ and core-shell $\text{NaYb}_{0.92}\text{Er}_{0.08}\text{F}_4@ \text{NaLu}_{1-x}\text{Yb}_x\text{F}_4$ ($x = 0, 0.25, 0.5, 0.75$ and 1) UCNP with various Yb^{3+} doping contents in the outermost shell. (i) Integrated emission enhancement of $\text{NaYb}_{0.92}\text{Er}_{0.08}\text{F}_4@ \text{NaLu}_{1-x}\text{Yb}_x\text{F}_4$ ($x = 0, 0.25, 0.5, 0.75$ and 1) sulfo-Cy3-UCNPs; the enhancements were obtained by calculating the ratio of UCL intensity of the sulfo-Cy3-UCNPs versus UCNP. (j) Normalized upconversion emission spectra of $\text{NaYb}_{0.92}\text{Er}_{0.08}\text{F}_4@ \text{NaLu}_{0.25}\text{Yb}_{0.75}\text{F}_4$ UCNP with and without sulfo-Cy3 at a dye concentration of $4.00 \mu\text{M}$ ($\lambda_{\text{ex}} = 980 \text{ nm}$, 63 W cm^{-2}). (k) Normalized upconversion emission spectra of $\text{NaYb}_{0.92}\text{Er}_{0.08}\text{F}_4@ \text{NaLuF}_4$ UCNP with and without sulfo-Cy3 at a dye concentration of $4.00 \mu\text{M}$ ($\lambda_{\text{ex}} = 980 \text{ nm}$, 63 W cm^{-2}). The emission intensity at 576 nm of sulfo-Cy3-UCNPs (the emission peak of sulfo-Cy3) in (i) and (j) was normalized to unity, respectively.

sulfo-Cy3-amine with a coordination group on the fluorescence core produced only a weak enhancement, and merely a faint emission peak from sulfo-Cy3-amine was observed in the upconversion spectra under 980 nm excitation (Fig. S8†). The weaker enhancement of sulfo-Cy3-amine was attributed to its poor solubility in chloroform. By adding the solvent DMSO into sulfo-Cy3-amine modified UCNP in CHCl_3 , a higher upconversion enhancement from FRET was achieved (Fig. S9†). Besides, the improved response of the decay kinetics of sulfo-RB-UCNPs also demonstrated the benefit of sulfo-rhodamine B as an acceptor for FRET (Fig. S10†). Sulfo-rhodamine B was used for further studies.

Larger-sized UCNP have a smaller surface-to-volume ratio than smaller UCNP, which typically leads to lower FRET

efficiency from UCNP to surface acceptors. To improve FRET-enhanced upconversion in larger-sized UCNP, we designed core-shell-shell UCNP with the formula $\text{NaYbF}_4@ \text{NaYb}_{0.92}\text{Er}_{0.08}\text{F}_4@ \text{NaLu}_{1-x}\text{Yb}_x\text{F}_4$ ($x = 0, 0.25, 0.5, 0.75, 1$) (Fig. 2a). The core was composed of NaYbF_4 enriched with sensitizer Yb^{3+} to augment excitation light absorption. We selected $\text{NaYb}_{0.92}\text{Er}_{0.08}\text{F}_4$ as the intermediate layer with a thickness of 5 nm, where the FRET donor Er^{3+} ions were localized near the particle surface, and then adopted a 2 nm thick protective shell of $\text{NaLu}_{1-x}\text{Yb}_x\text{F}_4$ to ensure its strong upconversion emission. TEM images showed the uniform size of the synthesized UCNP with a core diameter of $11.7 \pm 1.1 \text{ nm}$, a core and intermediate shell (core-shell) diameter of $20.9 \pm 0.8 \text{ nm}$,



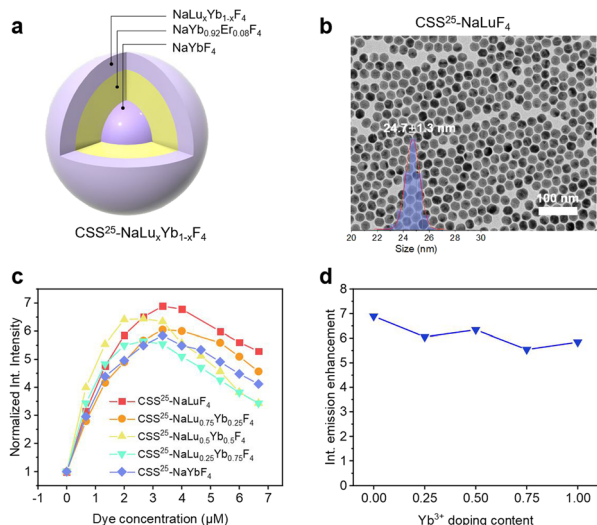


Fig. 2 FRET-enhanced upconversion of core-shell-shell UCNPs with 980 nm irradiation. (a) Schematic structure of core-shell-shell (CSS) UCNPs ($\text{NaYbF}_4@ \text{NaYb}_{0.92}\text{Er}_{0.08}\text{F}_4@ \text{NaLu}_{1-x}\text{Yb}_x\text{F}_4$) (b) TEM image and size distribution of the as-prepared CSS $\text{NaYbF}_4@ \text{NaYb}_{0.92}\text{Er}_{0.08}\text{F}_4@ \text{NaLuF}_4$ UCNPs. (c) Integrated UCL intensity of sulfo-RB-UCNPs ($\text{NaYbF}_4@ \text{NaYb}_{0.92}\text{Er}_{0.08}\text{F}_4@ \text{NaLu}_{1-x}\text{Yb}_x\text{F}_4$) ($x = 0, 0.25, 0.5, 0.75$ and 1) as a function of sulfo-rhodamine B concentration ($\lambda_{\text{ex}} = 980 \text{ nm}$, 63 W cm^{-2}); integrated intensities were normalized to the integrated intensity of UCNPs without sulfo-RB. (d) Integrated emission enhancement of sulfo-RB-CSS 25 - $\text{NaLu}_{1-x}\text{Yb}_x\text{F}_4$ with Yb^{3+} contents in the outermost shell varied from 0 to 1; the enhancements were obtained by calculating the ratio of integrated UCL intensity of the sulfo-RB-UCNPs versus the corresponding UCNPs.

and an entire core-shell-shell particle diameter of $\sim 25 \text{ nm}$ (Fig. 2b and S12[†]).

Then, we studied the effect of Yb^{3+} in the outermost shell on FRET-enhanced upconversion. Remarkably, in contrast to the Yb^{3+} doping-dependent enhancement in smaller particles, the enhancement in larger particles was independent of Yb^{3+} ion doping concentration and all particles had similar titration curves upon the addition of sulfo-rhodamine B (Fig. 2c, d, S13 and S14[†]). Notably, there was a brief saturation plateau during dye titration. At this stage, the augmentation in dye concentration induced an elevation in FRET-enhanced upconversion, which was offset by a reduction in emission due to deleterious dye-dye interactions. Consequently, the integrated upconversion emission changes were not markedly pronounced within this concentration range. The saturation points of all UCNPs for dye titrations were in the concentration range of $2.67\text{--}3.33 \mu\text{M}$, with variations lying within the margin of experimental error (Fig. 2c). Around six times upconversion enhancement was achieved in all the large CSS UCNPs with the addition of sulfo-rhodamine B (Fig. 2d). We attributed this to the sufficient number of Yb^{3+} ions in the inner core-shell layer that could capture excitation light and transfer it to Er^{3+} , resulting in the saturation of the photon-accepting ability of Er^{3+} ions. Therefore, Yb^{3+} ions in the active shell had a negligible effect on enhancing the population of excited Er^{3+} ions and the FRET-enhanced upconversion. We also employed sulfo-Cy3 as

a FRET acceptor for the bigger UCNPs. The upconversion enhancement was also insensitive to Yb^{3+} doping (Fig. S15[†]). For the smaller UCNPs decorated with sulfo-rhodamine B, the enhancement depended on the Yb^{3+} doping, which was consistent with the sulfo-Cy3-UCNP systems (Fig. S16[†]). It is worth noting that there is a saturation point for the dye concentration in the dye titration experiments. Beyond this point, the integrated upconversion intensity diminished (Fig. 2c), which was attributed to deleterious dye-dye interactions (*i.e.* cross-relaxation) on the nanoparticle surface.⁴³ Moreover, as the dye concentration increased, a more pronounced inner-filter effect (absorption of the light emitted by the sulfo-Cy3 molecules present at high concentration due to their own absorption) also caused a decrease in dye intensity and an apparent red shift of the emission^{44,48} (Fig. S13[†]).

To further demonstrate the importance of the protective shell, we additionally synthesized UCNPs without NaLuF_4 -shell coating ($\text{NaYbF}_4@ \text{NaYb}_{0.92}\text{Er}_{0.08}\text{F}_4@ \text{NaYb}_{0.92}\text{Er}_{0.08}\text{F}_4$, denoted as CSS 25 - $\text{NaYb}_{0.92}\text{Er}_{0.08}\text{F}_4$) (Fig. S17[†]). Compared with the NaLuF_4 coated UCNPs (CSS 25 - NaLuF_4), the UCNPs without a protective shell exhibited considerably lower upconversion brightness. With the addition of sulfo-rhodamine B, CSS 25 - $\text{NaYb}_{0.92}\text{Er}_{0.08}\text{F}_4$ and CSS 25 - NaLuF_4 UCNPs showed 3.3-fold and 6.2-fold enhancement, respectively (Fig. S18a and b[†]). The lower upconversion enhancement and dim upconversion brightness of CSS 25 - $\text{NaYb}_{0.92}\text{Er}_{0.08}\text{F}_4$ illustrated that the surface quenching stemming from the $\text{NaYb}_{0.92}\text{Er}_{0.08}\text{F}_4$ layer was more dominant than the FRET-enhanced upconversion and the protective shell was imperative for constructing bright upconversion probes. Fig. S18c and d[†] present the luminescence kinetic response of CSS 25 - $\text{NaYb}_{0.92}\text{Er}_{0.08}\text{F}_4$ and CSS 25 - NaLuF_4 UCNPs to the addition of acceptor sulfo-Cy3 dye, and the less sensitive decay kinetic response of CSS 25 - $\text{NaYb}_{0.92}\text{Er}_{0.08}\text{F}_4$ UCNPs also proved the significance of the protective shell.

Furthermore, we modified the amphiphilic polymer DSPE-mPEG on the surface of UCNPs through hydrophobic interactions to render the UCNPs hydrophilic, named DSPE-UCNPs. As depicted in Fig. S19,[†] the DSPE-UCNPs remained well-dispersed in a hydrophilic environment. By directly mixing sulfo-rhodamine B and DSPE-UCNPs (termed DSPE-Sulfo-RB-UCNPs), a 2.5-fold upconversion enhancement was achieved (Fig. 3b). DSPE-Sulfo-RB-UCNPs still preserved their good dispersion after the addition of sulfo-rhodamine B (Fig. 3a and S19[†]). Remarkably, after modification with DSPE-mPEG, the upconversion enhancement of DSPE-UCNPs was lower than that of OA-UCNPs (as-synthesized OA-coordinated UCNPs without surface modification), which was ascribed to the surface-covered DSPE-mPEG further increasing the D-A distance between UCNPs and dye.⁴⁹ Despite this adverse effect on FRET, surface modification of UCNPs is essential for potential future bioassays.

Fig. S21 and S22[†] present the emission kinetic response curves of CSS-UCNPs and DSPE-CSS-UCNPs before and after addition of the dyes sulfo-rhodamine B. The response of the donor Er^{3+} emission decay lifetime did not change significantly with the doping of Yb^{3+} in the outermost shell, which was in agreement with the steady-state spectral results and could be



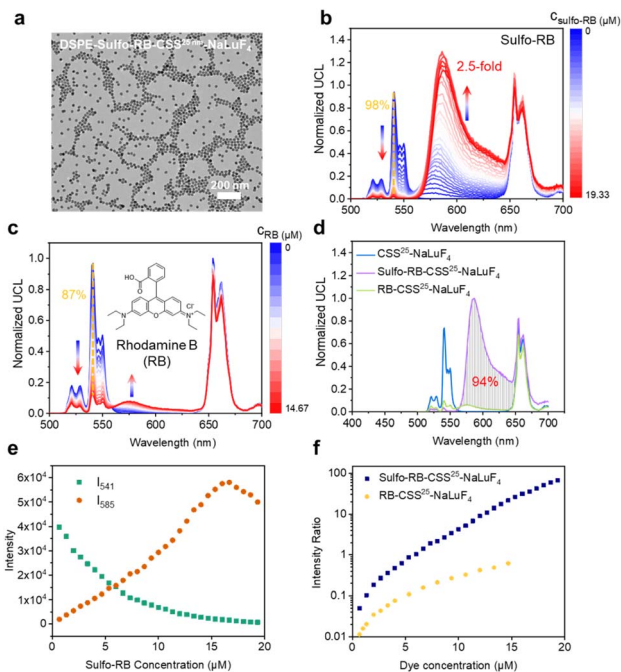


Fig. 3 FRET-enhanced upconversion in DSPE-UCNPs. (a) TEM images of DSPE-Sulfo-RB-CSS²⁵-NaLuF₄ dispersed in ethanol. (b) Emission spectra of DSPE-Sulfo-RB-CSS²⁵-NaLuF₄ in ethanol with the sulfo-rhodamine B concentration varied from 0 to 19.33 μM. (c) Emission spectra of DSPE-RB-CSS²⁵-NaLuF₄ in ethanol with the sulfo-rhodamine B concentration varied from 0 to 14.67 μM, (inset) the molecular structure of rhodamine B (RB), and the emission intensity at 654 nm of DSPE-CSS²⁵-NaLuF₄ (the red emission peak of Er³⁺) in (b) and (c) was normalized to unity, respectively. Note: the gradient arrows indicate the trend of the spectral peak as a function of concentration. (d) The UCL spectra of DSPE-UCNPs (blue), DSPE-Sulfo-RB-CSS²⁵-NaLuF₄ (purple, 18.00 μM sulfo-rhodamine B) and DSPE-RB-CSS²⁵-NaLuF₄ (green, 14.67 μM rhodamine B) upon excitation at 980 nm (63 W cm⁻² irradiance), and the emission intensity at 587 nm of DSPE-Sulfo-RB-CSS²⁵-NaLuF₄ (the emission peak of Sulfo-RB) was normalized to unity, respectively. (e) The intensity of the emission peak of sulfo-rhodamine B at 585 nm and the green emission peak of Er³⁺ in the DSPE-Sulfo-RB-UCNP system (ethanol) with the concentration of sulfo-rhodamine B varied from 0 to 19.33 μM. (f) The corresponding I₅₈₅/I₅₄₁ and I₅₇₇/I₅₄₁ ratio versus the sulfo-rhodamine B concentration of DSPE-Sulfo-RB-UCNPs and rhodamine B concentration of DSPE-RB-UCNPs, respectively.

attributed to the energy storage in the Yb³⁺ network. Both CSS-UCNPs and DSPE-CSS-UCNPs had a relatively insignificant luminescence kinetic response, which was due to the increased D–A distance caused by the presence of the shell layer and the rapid charging of the donor Er³⁺ from the Yb³⁺ network. In addition, the back energy transfer (BET) from Er³⁺ to Yb³⁺ would also lead to an insignificant luminescence kinetic response of UCNPs. Notably, we used a long excitation pulse length from a TTL-controlled CW laser diode, by using which the energy was accumulated in the sensitizer Yb³⁺ network, reducing the response of the decay kinetics. Therefore, the decay times were less sensitive to the addition of the dye acceptor molecules.⁴⁴

To substantiate that the upconversion emission by sulfo-rhodamine B stems from effective FRET, we drew

comparisons with rhodamine B, whose absorption maximum at 542 nm ideally overlaps with the UCNP emission spectrum (Fig. S23[†]), but lacks the sulfate coordination groups presented in sulfo-rhodamine B. Despite the spectral match, rhodamine B mixed with DSPE-UCNPs led to only a weak upconversion emission of rhodamine B (illustrated in Fig. 3c), even with a noticeable quenching of Er³⁺'s green emission (87%). Besides, the luminescence kinetic response of rhodamine B-UCNPs was less significant than that of sulfo-rhodamine B-UCNPs (Fig. S24[†]). These results suggest that rhodamine B does not successfully anchor to the DSPE-UCNP surface and primarily relies on less efficient reabsorption processes for energy transfer from the UCNPs to the dye. In contrast, when we used sulfo-rhodamine B, which can coordinate to the surface of UCNPs, the short D–A distance facilitated an efficient FRET process. The green emission of sulfo-rhodamine B-UCNPs was quenched by 93%, which was similar to that of rhodamine B-UCNPs, but the dye emission was greatly enhanced by FRET. Moreover, the total emission of sulfo-rhodamine B-UCNPs also increased. Based on these results, we conclude that the total emission of FRET-enhanced upconversion will decrease when photon reabsorption prevails. In sulfo-rhodamine B-UCNPs, although we cannot rule out the role of photon reabsorption, the increased emission of the dye and the total photons collected are mainly attributed to FRET. Furthermore, the enhanced luminescence kinetic response of UCNPs by using sulfo-rhodamine B compared to that by using rhodamine B also corroborated the crucial role of FRET (Fig. S24[†]).

Interestingly, as the sulfo-rhodamine B concentration increased from 0.67 μM to 19.33 μM, the green emission of DSPE-UCNPs was markedly quenched (98%, Fig. 3b and e), and the ratio of the emission peak of sulfo-rhodamine B at 585 nm to the green emission peak of Er³⁺ at 541 nm varied from 0.050 to 67, spanning three orders of magnitude (Fig. 3f). Owing to the poor enhancement of rhodamine B, the ratio of the emission peak of rhodamine B at 577 nm to the green emission peak of Er³⁺ at 541 nm exhibited a smaller slope with respect to the dye concentration, and only varied from 0.016 to 0.62. Besides, a good linear correlation between the I₅₈₅/I₅₄₁ ratio and sulfo-rhodamine B concentration was observed in the dye concentration range of 1.33–16.00 μM. This high dye concentration-dependent ratio of the DSPE-Sulfo-RB-UCNP system demonstrated its potential for detection.

To examine the potential of DSPE-Sulfo-RB-UCNPs as single-particle imaging probes, we investigated the FRET-enhanced upconversion at the single-particle level. We chose inert-shelled CSS UCNPs for single-particle studies due to their high UCL brightness and FRET-based upconversion enhancement. Single-particle samples of DSPE-Sulfo-RB-UCNPs were prepared by stepwise drop-casting of DSPE-UCNPs and sulfo-rhodamine B in ethanol onto a coverslip, and then imaging by wide-field microscopy (Fig. S26[†]). Fig. 4a–e show single-particle data of DSPE-UCNPs and DSPE-Sulfo-RB-UCNPs, showing an overall 2.2-fold UCL enhancement under 976 nm irradiation. The single-particle wide field images were further colocalized by scanning electron microscopy (SEM) to confirm the emission



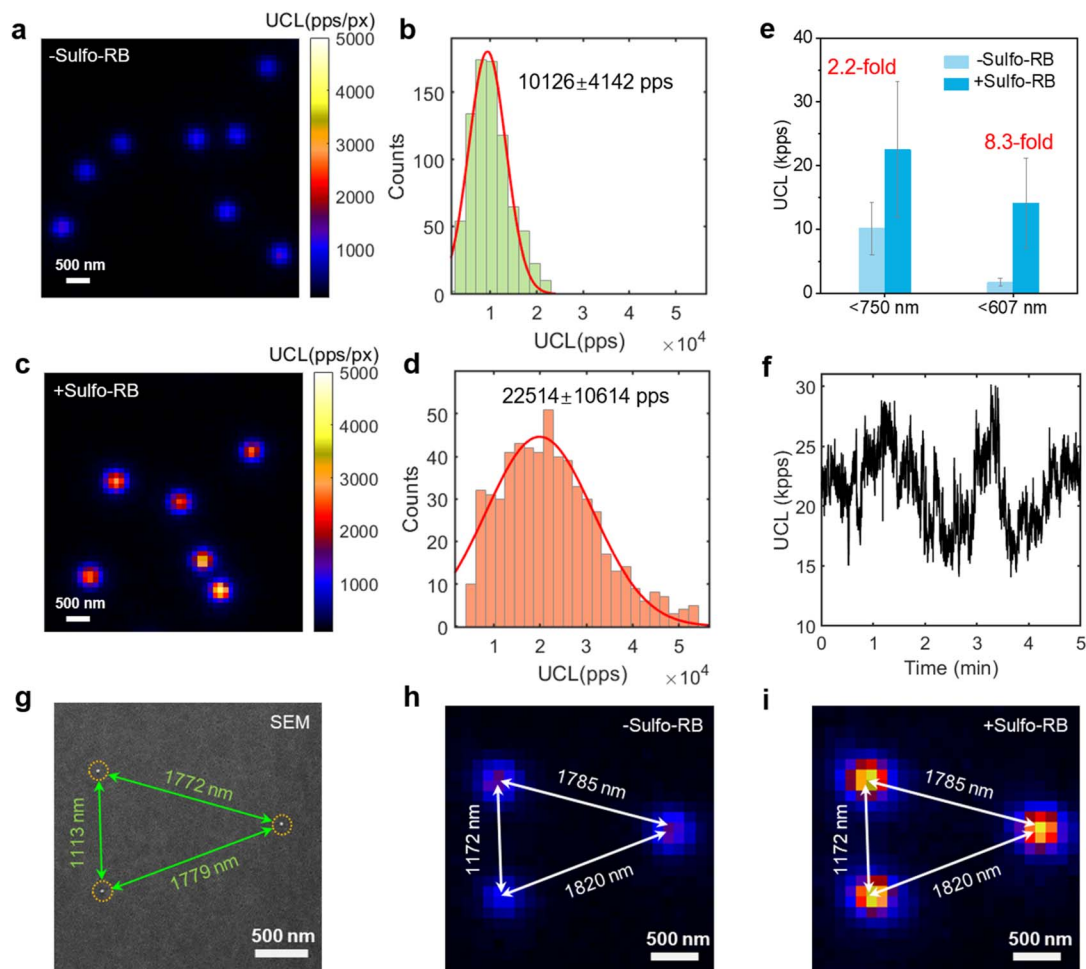


Fig. 4 Single-particle upconversion enhancement of DSPE-UCNPs by using sulfo-rhodamine B. (a) Representative single-particle image and corresponding (b) single-particle UCL histogram of DSPE-CSS²⁵-NaLuF₄ under 976 nm excitation (11.6 kW cm⁻²). (c) Representative single-particle image and corresponding (d) single-particle UCL histograms of DSPE-Sulfo-RB-CSS²⁵-NaLuF₄ under 976 nm excitation (11.6 kW cm⁻²). (e) The single-particle intensity of DSPE-CSS²⁵-NaLuF₄ and DSPE-Sulfo-RB-CSS²⁵-NaLuF₄ under 976 nm excitation (11.6 kW cm⁻²). (Left) 750 nm short pass, (right) 607 nm short pass. (f) Time-dependent emission intensity changes of DSPE-Sulfo-RB-CSS²⁵-NaLuF₄ from single-particle measurement under the irradiation of a 976 nm laser (duration: 5 min, irradiance: 11.6 kW cm⁻²). (g) Colocalization of particles using SEM. Corresponding wide-field UCL images at 11.6 kW cm⁻² of (h) DSPE-CSS²⁵-NaLuF₄ and (i) DSPE-Sulfo-RB-CSS²⁵-NaLuF₄. Scale bars, 500 nm.

from individual particles and intuitively show the emission enhancement of individual particles (Fig. 4g–i).

In the bulk spectral measurement, the red emission of UCNPs remains unchanged with the addition of a dye (Fig. 3b). Hence, the red emission intensity of UCNPs could be regarded as a constant value in both of DSPE-UCNPs and DSPE-Sulfo-RB-UCNPs. After subtracting the red emission, the single-particle green emission (<607 nm) intensity of DSPE-UCNPs and DSPE-Sulfo-RB-UCNPs was 1702 pps and 14 090 pps, respectively, achieving an 8.3-fold enhancement (Fig. 4e). It is worth noting that the single-particle UCL intensity of DSPE-Sulfo-RB-UCNPs has excellent stability under 976 nm irradiation of 11.6 kW cm⁻² (Fig. 4f). Due to the possible departure, coordination or photobleaching of sulfo-rhodamine B on the surface of UCNPs, the single-particle emission of DSPE-Sulfo-RB-UCNPs fluctuated with the irradiation time. The time-dependent brightness of 29 individual UCNPs was analysed, and the UCL

intensity only decreased to $84.9 \pm 38.7\%$ on average after 5 minutes of 976 nm laser irradiation at 11.6 kW cm⁻².

3 Conclusion

In conclusion, we successfully achieved enhanced brightness in single-particle upconversion through FRET by meticulously optimizing the size and structures of UCNPs, and organic dye species. We observed that for smaller UCNPs, approximately 14 nm in size, a greater concentration of Yb³⁺ ions in the outermost layer significantly bolstered the FRET-based upconversion enhancement. Conversely, for larger UCNPs, around 25 nm in size, where more Yb³⁺ ions reside in the inner layer, the effect of additional outermost Yb³⁺ ions on FRET efficiency was marginal. Commercially available fluorescent dyes, sulfo-Cy3, sulfo-Cy3-amine and sulfo-rhodamine B were used as FRET acceptors to enhance the emission from UCNPs, and



sulfo-rhodamine B outperformed the others. A simple complexation of amphiphilic polymer DSPE-mPEG modified UCNPs with sulfo-rhodamine B led to a 2.2-fold enhancement in upconversion in a hydrophilic environment. Furthermore, this complexation resulted in an 8.3-fold increase in single-particle FRET-enhanced green emission. Remarkably, the DSPE-sulfo-RB-UCNP assembly demonstrated a sensitive response to dye concentration, suggesting that these single-particle probes with FRET-enhanced upconversion can offer not only brighter emissions but also the capability for single-particle detection. Capitalizing on these findings, our study provides crucial insights for developing high-brightness, high-sensitivity, and high-stability upconversion probes tailored for biological applications, particularly in the realm of single-molecule detection.^{3,50–52}

4 Experimental

4.1 Nanoparticle synthesis procedure and characterization

4.1.1 Reagents. 1-Octadecene (ODE) (>90%), oleic acid (OA) (>90%) and sulfo-rhodamine B were purchased from Sigma-Aldrich, sulfo-Cy3-amine was purchased from Duofluor and rhodamine B was purchased from Shanghai Yuanye Biotechnology Co., Ltd. $\text{YbCl}_3 \cdot 6\text{H}_2\text{O}$ (99.99%), $\text{ErCl}_3 \cdot 6\text{H}_2\text{O}$ (99.99%), $\text{LuCl}_3 \cdot 6\text{H}_2\text{O}$ (99.99%), and dimethylsulfoxide (DMSO), were purchased from Shanghai Aladdin Biochemical Technology Co., sodium oleate was purchased from TCI, and other reagents such as NH_4F , NaOH, ethanol, methanol, cyclohexane, and chloroform (CHCl_3) were purchased from Sinopharm Chemical Reagent Co., China. DSPE-mPEG (~2000) was purchased from Melo PEG, poly-L-lysine was purchased from Solarbio. All chemical reagents were of analytical grade and were used directly without further purification.

4.1.2 Synthesis of an ~10 nm $\text{NaYb}_{0.92}\text{Er}_{0.08}\text{F}_4$ core. A mixture of 1 mmol (1 mL, 1 M) water solution of the corresponding lanthanide chloride (YbCl_3 : 0.92 mmol and ErCl_3 : 0.08 mmol), 10 mL oleic acid and 10 mL 1-octadecene was added to a 100 mL flask. The mixture was stirred under a nitrogen atmosphere and heated to 160 °C for 1 h to remove the water. Then, the mixture was cooled to 50 °C, and 0.34 g NH_4F and 2.03 g sodium oleate were quickly added into the reaction. The solution was heated to 110–120 °C for 30 min and degassed for another 30 min; the solution was heated to 290 °C and kept for 50 min before cooling down to room temperature. The as-prepared nanoparticles were precipitated by using additional 20 mL ethanol, and the resulting mixture was centrifugally separated (15 000 rpm for 10 min) to obtain a compact pellet, and the supernatant was discarded. The products were collected and washed with cyclohexane and ethanol (40 mL, 1 : 1, v/v) three times. The UCNPs (diameter 10.1 nm \pm 1.0 nm) were stored in 10 mL cyclohexane to be used for shell coating.

4.1.3 Synthesis of ~14 nm core-shell $\text{NaYb}_{0.92}\text{Er}_{0.08}\text{F}_4$ @- $\text{NaLu}_{1-x}\text{Yb}_x\text{F}_4$ ($x = 0, 0.25, 0.5, 0.75, 1$). The shell precursor was first prepared by mixing 0.1 mL (0.1 mmol) water solution of the corresponding lanthanide chloride (1 M) with 3 mL oleic acid and 8 mL 1-octadecene in a 100 mL flask. The mixture was

stirred under a nitrogen atmosphere and heated to 160 °C for 40 min to remove the water. After cooling down to 50 °C, 0.1 mL of the prepared ~10 nm $\text{NaYb}_{0.92}\text{Er}_{0.08}\text{F}_4$ core in cyclohexane and 1.25 mL methanol solution containing NH_4F (0.375 mmol) and NaOH (0.25 mmol) were added and stirred at 50 °C for 30 min. The resultant solution was heated at 120 °C for 30 min and degassed for another 30 min under vacuum to remove low-boiling solvents, and then heated to 290 °C and maintained for 30 min under a nitrogen atmosphere. The subsequent purification steps are the same as used for ~10 nm $\text{NaYb}_{0.92}\text{Er}_{0.08}\text{F}_4$ UCNPs described above. The product was stored in 5 mL cyclohexane.

4.1.4 Synthesis of an ~11 nm NaYbF_4 core. The synthesis steps are the same as used for ~10 nm $\text{NaYb}_{0.92}\text{Er}_{0.08}\text{F}_4$ core UCNPs described above, expect that the added lanthanide chloride is 1 mmol YbCl_3 water solution.

4.1.5 Synthesis of ~21 nm core-shell NaYbF_4 @- $\text{NaYb}_{0.92}\text{Er}_{0.08}\text{F}_4$. The shell precursor was first prepared by mixing 1.2 mmol (1.2 mL, 1 M) water solution of the corresponding lanthanide chloride (YbCl_3 : 1.104 mmol and ErCl_3 : 0.096 mmol) with 9 mL oleic acid and 24 mL 1-octadecene in a 100 mL flask. The mixture was stirred under a nitrogen atmosphere and heated to 160 °C for 60 min to remove the water. After cooling down to 50 °C, 3 mL prepared ~11 nm NaYbF_4 core in cyclohexane and 15 mL methanol solution containing NH_4F (4.5 mmol) and NaOH (3 mmol) were added and stirred at 50 °C for 30 min. The resultant solution was heated at 120 °C for 30 min and degassed for another 30 min under vacuum to remove low-boiling solvents, and then heated to 290 °C and maintained for 50 min under a nitrogen atmosphere. The subsequent purification steps are the same as those used for ~10 nm $\text{NaYb}_{0.92}\text{Er}_{0.08}\text{F}_4$ UCNPs described above. The product was stored in 10 mL cyclohexane.

4.1.6 Synthesis of ~25 nm core-shell-shell NaYbF_4 @- $\text{NaYb}_{0.92}\text{Er}_{0.08}\text{F}_4$ @- $\text{NaLu}_{1-x}\text{Yb}_x\text{F}_4$ ($x = 0, 0.25, 0.5, 0.75, 1$). The shell precursor was first prepared by mixing 0.1 mL (0.1 mmol) water solution of the corresponding lanthanide chloride (1 M) with 3 mL oleic acid and 8 mL 1-octadecene in a 100 mL flask. The mixture was stirred under a nitrogen atmosphere and heated to 160 °C for 40 min to remove the water. After cooling down to 50 °C, 1 mL prepared ~21 nm core-shell NaYbF_4 @- $\text{NaYb}_{0.92}\text{Er}_{0.08}\text{F}_4$ in cyclohexane and 1.25 mL methanol solution containing NH_4F (0.375 mmol) and NaOH (0.25 mmol) were added and stirred at 50 °C for 30 min. The resultant solution was heated at 120 °C for 30 min and degassed for another 30 min under vacuum to remove low-boiling solvents, and then heated to 290 °C and maintained for 45 min under a nitrogen atmosphere. The subsequent purification steps are the same as those used for ~10 nm $\text{NaYb}_{0.92}\text{Er}_{0.08}\text{F}_4$ UCNPs described above. The product was stored in 5 mL cyclohexane.

4.1.7 Nanoparticle characterization. Powder XRD of the UCNPs powders was performed on a Bruker D2 diffractometer at a scanning rate of 5° min^{-1} in the 2θ range from 10° to 75°. The luminescence emission spectra were recorded on an Edinburgh FLS1000 luminescence spectrometer (Edinburgh Instruments) with an external 980 nm laser. The size, morphology, and dispersibility of nanocomposites were recorded on a TEM (Hitachi



HT7800) at an acceleration voltage of 100 kV. The TEM sample was prepared by dripping a UCNP cyclohexane solution onto a carbon-coated copper grid and then drying the grid at room temperature. All the photoluminescence studies were carried out at room temperature.

4.2 Sample preparation for dye titration measurements

4.2.1 Direct ligand-exchange reaction of UCNPs. The as-prepared UCNP dispersion in cyclohexane (0.5 mL, 0.38 μM of ~ 25 nm CSS UCNPs and 1.9 μM of ~ 14 nm CS UCNPs) was centrifuged to separate the UCNPs from the solution (15 000 rpm for 15 min) and re-dispersed in 3 mL of chloroform. Then, the above-prepared UCNPs (1.5 mL) in chloroform were mixed with 0, 1, 2, 3, 4, 5, ... μL of dye solution (1 mM dye in chloroform/DMSO (2 : 1)), respectively. The solution was stirred for 2 min and the luminescence was measured under 980 nm irradiation (63 W cm^{-2}).

4.2.2 Dye titration in DSPE-UCNPs. The as-prepared OA-capped $\text{NaYbF}_4@ \text{NaYb}_{0.92}\text{Er}_{0.08}\text{F}_4@ \text{NaLuF}_4$ UCNPs (0.5 mL, 0.38 μM) were mixed with a chloroform solution (6 mL) containing 4 mg DSPE-mPEG (~ 2000) in a 50 mL flask. The mixture was stirred for 30 min and the solvent is removed by rotary evaporation (30°C) to obtain a film. Then the film was hydrated with deionized water (2 mL), and the UCNPs became soluble after vigorous sonication. The solution was transferred to a microtube and centrifuged lightly (1000 rpm, 5 min), and the sediment was discarded to remove possible large aggregates. Excess DSPE-mPEG was purified from DSPE-UCNPs by centrifugation (15 000 rpm, 10 min) and washing. The DSPE-UCNPs were dispersed in 6 mL ethanol. Then, the above-prepared DSPE-UCNPs (31.6 nM, 1.5 mL) in ethanol were mixed with 0, 1, 2, 3, 4, 5, ... μL of dye sulfo-rhodamine B solution (1 mM sulfo-rhodamine B in ethanol), respectively. The solution was stirred for 2 min and the luminescence was measured under 980 nm irradiation (63 W cm^{-2}).

4.2.3 Calculation of the integrated emission enhancement factor of FRET-enhanced upconversion. The integrated emission enhancement factors were calculated by using the following equation:

$$N = \frac{F_{\text{dye-UCNPs}}}{F_{\text{UCNPs}}}$$

where $F_{\text{dye-UCNPs}}$ and F_{UCNPs} are integrated areas of the emission spectra of the dye-UCNPs and UCNPs.

4.2.4 Calculation of Er^{3+} 's green emission quenching. The Er^{3+} 's green emission quenching ratio was obtained by calculating the ratio of Er^{3+} 's emission intensity at 541 nm of dye-UCNPs and UCNPs.

4.2.5 Sample preparation for single-particle measurements. Clean coverslips were pre-coated with 1% (w/v) poly-L-lysine, approximately 200 μL poly-L-lysine solution was drop-cast onto the coverslip, and after 1 min incubation, cyclohexane was used to wash the excess poly-L-lysine. The cyclohexane was allowed to evaporate and when the coverslip was dry, approximately 100 μL moderately diluted DSPE-UCNPs (2000 \times) in ethanol was drop-cast onto the coverslip, and after

1 min incubation, the excess DSPE-UCNPs were washed with 1 mL ethanol 5 times. After the evaporation of ethanol and when the coverslip was dry, approximately 100 μL 0.01 mM sulfo-rhodamine B in ethanol was drop-cast onto the coverslip. After the evaporation of ethanol, sulfo-rhodamine B was coated on UCNPs. Then, the coverslip was attached to a microscope slide using double-sided tape with a window.

Author contributions

J. H. synthesized inorganic nanoparticles, obtained FRET-enhanced upconversion results and carried out the single-nanoparticle measurement. Q. L. and J. H. prepared the manuscript, and all authors discussed and commented on the manuscript. The manuscript was written through contributions of all authors. All authors have given approval to the final version of the manuscript.

Conflicts of interest

The authors declare no conflict of interest.

Acknowledgements

This work was financially supported by the National Key Research and Development Program of China (Grant No. 2022YFB3503700) and National Natural Science Foundation of China (Grant No. 22074021 and No. 22174025).

References

- 1 M. Saqib, M. Zafar, M. I. Halawa, S. Murtaza, G. M. Kamal and G. Xu, *ACS Meas. Sci. Au*, 2023, **4**, 3–24.
- 2 D. R. Walt, *Anal. Chem.*, 2013, **85**, 1258–1263.
- 3 J. J. Gooding and K. Gaus, *Angew Chem. Int. Ed. Engl.*, 2016, **55**, 11354–11366.
- 4 N. Akkilic, S. Geschwindner and F. Hook, *Biosens. Bioelectron.*, 2020, **151**, 111944.
- 5 M. Holzinger, A. Le Goff and S. Cosnier, *Front. Chem.*, 2014, **2**, 63.
- 6 D. Jin, P. Xi, B. Wang, L. Zhang, J. Enderlein and A. M. van Oijen, *Nat. Methods*, 2018, **15**, 415–423.
- 7 S. Nie and S. R. Emory, *Science*, 1997, **275**, 1102–1106.
- 8 C. Joo, H. Balci, Y. Ishitsuka, C. Buranachai and T. Ha, *Annu. Rev. Biochem.*, 2008, **77**, 51–76.
- 9 Y. Sako, S. Minoghchi and T. Yanagida, *Nat. Cell Biol.*, 2000, **2**, 168–172.
- 10 A. B. Taylor and P. Zijlstra, *ACS Sens.*, 2017, **2**, 1103–1122.
- 11 A. B. Zrimsek, N. Chiang, M. Mattei, S. Zaleski, M. O. McAnally, C. T. Chapman, A. I. Henry, G. C. Schatz and R. P. Van Duyne, *Chem. Rev.*, 2017, **117**, 7583–7613.
- 12 J. N. Anker, W. P. Hall, O. Lyandres, N. C. Shah, J. Zhao and R. P. Van Duyne, *Nat. Mater.*, 2008, **7**, 442–453.
- 13 H. Mazal and G. Haran, *Curr. Opin. Biomed. Eng.*, 2019, **12**, 8–17.
- 14 C. Y. Zhang, H. C. Yeh, M. T. Kuroki and T. H. Wang, *Nat. Mater.*, 2005, **4**, 826–831.



- 15 W. B. Asher, P. Geggier, M. D. Holsey, G. T. Gilmore, A. K. Pati, J. Meszaros, D. S. Terry, S. Mathiasen, M. J. Kaliszewski, M. D. McCauley, A. Govindaraju, Z. Zhou, K. G. Harikumar, K. Jaqaman, L. J. Miller, A. W. Smith, S. C. Blanchard and J. A. Javitch, *Nat. Methods*, 2021, **18**, 397–405.
- 16 R. Roy, S. Hohng and T. Ha, *Nat. Methods*, 2008, **5**, 507–516.
- 17 W. R. Algar, N. Hildebrandt, S. S. Vogel and I. L. Medintz, *Nat. Methods*, 2019, **16**, 815–829.
- 18 C. Eggeling, J. Widengren, L. Brand, J. Schaffer, S. Felekyan and C. A. Seidel, *J. Phys. Chem. A*, 2006, **110**, 2979–2995.
- 19 A. Hlavacek, Z. Farka, M. Hubner, V. Hornakova, D. Nemecek, R. Niessner, P. Skladal, D. Knopp and H. H. Gorris, *Anal. Chem.*, 2016, **88**, 6011–6017.
- 20 S. H. Nam, Y. M. Bae, Y. I. Park, J. H. Kim, H. M. Kim, J. S. Choi, K. T. Lee, T. Hyeon and Y. D. Suh, *Angew Chem. Int. Ed. Engl.*, 2011, **50**, 6093–6097.
- 21 F. Wang, S. Wen, H. He, B. Wang, Z. Zhou, O. Shimoni and D. Jin, *Light: Sci. Appl.*, 2018, **7**, 18007.
- 22 J. Zhou, C. Li, D. Li, X. Liu, Z. Mu, W. Gao, J. Qiu and R. Deng, *Nat. Commun.*, 2020, **11**, 4297.
- 23 H. Li, X. Wang, T. Y. Ohulchanskyy and G. Chen, *Adv. Mater.*, 2021, **33**, 2000678.
- 24 X. Cheng, D. Tu, W. Zheng and X. Chen, *Chem. Commun.*, 2020, **56**, 15118–15132.
- 25 F. Auzel, *Chem. Rev.*, 2004, **104**, 139–173.
- 26 G. Chen, H. Qiu, P. N. Prasad and X. Chen, *Chem. Rev.*, 2014, **114**, 5161–5214.
- 27 J. Zhou, Q. Liu, W. Feng, Y. Sun and F. Li, *Chem. Rev.*, 2015, **115**, 395–465.
- 28 X. Li, F. Zhang and D. Zhao, *Chem. Soc. Rev.*, 2015, **44**, 1346–1378.
- 29 F. Wang and X. Liu, *Chem. Soc. Rev.*, 2009, **38**, 976–989.
- 30 S. Wu, G. Han, D. J. Milliron, S. Aloni, V. Altoe, D. V. Talapin, B. E. Cohen and P. J. Schuck, *Proc. Natl. Acad. Sci. U. S. A.*, 2009, **106**, 10917–10921.
- 31 G. Chen, J. Shen, T. Y. Ohulchanskyy, N. J. Patel, A. Kutikov, Z. Li, J. Song, R. K. Pandey, H. Agren, P. N. Prasad and G. Han, *ACS Nano*, 2012, **6**, 8280–8287.
- 32 Q. Liu, Y. Sun, T. Yang, W. Feng, C. Li and F. Li, *J. Am. Chem. Soc.*, 2011, **133**, 17122–17125.
- 33 K. Malhotra, R. Fuku, B. Kumar, D. Hrovat, J. Van Houten, P. A. E. Piuonno, P. T. Gunning and U. J. Krull, *Nano Lett.*, 2022, **22**, 7285–7293.
- 34 H. Ge, D. Wang, Y. Pan, Y. Guo, H. Li, F. Zhang, X. Zhu, Y. Li, C. Zhang and L. Huang, *Angew Chem. Int. Ed. Engl.*, 2020, **59**, 8133–8137.
- 35 Z. Sun, H. Huang, R. Zhang, X. Yang, H. Yang, C. Li, Y. Zhang and Q. Wang, *Nano Lett.*, 2021, **21**, 6576–6583.
- 36 S. Chen, A. Z. Weitemier, X. Zeng, L. He, X. Wang, Y. Tao, A. J. Y. Huang, Y. Hashimoto-dani, M. Kano, H. Iwasaki, L. K. Parajuli, S. Okabe, D. B. L. Teh, A. H. All, I. Tsutsui-Kimura, K. F. Tanaka, X. Liu and T. J. McHugh, *Science*, 2018, **359**, 679–684.
- 37 Y. Liu, Y. Liu, W. Bu, C. Cheng, C. Zuo, Q. Xiao, Y. Sun, D. Ni, C. Zhang, J. Liu and J. Shi, *Angew Chem. Int. Ed. Engl.*, 2015, **54**, 8105–8109.
- 38 Y. Dai, H. Xiao, J. Liu, Q. Yuan, P. Ma, D. Yang, C. Li, Z. Cheng, Z. Hou, P. Yang and J. Lin, *J. Am. Chem. Soc.*, 2013, **135**, 18920–18929.
- 39 C. Chen, M. Song, Y. Du, Y. Yu, C. Li, Y. Han, F. Yan, Z. Shi and S. Feng, *Nano Lett.*, 2021, **21**, 5522–5531.
- 40 Y. Pan, J. Yang, X. Luan, X. Liu, X. Li, J. Yang, T. Huang, L. Sun, Y. Wang, Y. Lin and Y. Song, *Sci. Adv.*, 2019, **5**, eaav7199.
- 41 M. Xue, C. Cao, X. Zhou, M. Xu, W. Feng and F. Li, *Inorg. Chem.*, 2019, **58**, 14490–14497.
- 42 C. Siefe, R. D. Mehlenbacher, C. S. Peng, Y. Zhang, S. Fischer, A. Lay, C. A. McLellan, A. P. Alivisatos, S. Chu and J. A. Dionne, *J. Am. Chem. Soc.*, 2019, **141**, 16997–17005.
- 43 M. D. Wisser, S. Fischer, C. Siefe, A. P. Alivisatos, A. Salleo and J. A. Dionne, *Nano Lett.*, 2018, **18**, 2689–2695.
- 44 A. M. Kotulska, A. Pilch-Wrobel, S. Lahtinen, T. Soukka and A. Bednarkiewicz, *Light: Sci. Appl.*, 2022, **11**, 256.
- 45 J. Hu, D. Guan, B. Zhao, Y. Zhang, X. Qiu, Y. Zhang and Q. Liu, *Adv. Opt. Mater.*, 2022, **10**, 2101763.
- 46 Q. Liu, Y. Zhang, C. S. Peng, T. Yang, L. M. Joubert and S. Chu, *Nat. Photonics*, 2018, **12**, 548–553.
- 47 J. Hu, B. Zhao, R. Wen, X. Zhang, Y. Zhang, D. S. Kohane and Q. Liu, *Nano Lett.*, 2023, **23**, 5209–5216.
- 48 A. Pilch-Wrobel, A. M. Kotulska, S. Lahtinen, T. Soukka and A. Bednarkiewicz, *Small*, 2022, **18**, 2200464.
- 49 F. Pini, L. Frances-Soriano, V. Andriago, M. M. Natile and N. Hildebrandt, *ACS Nano*, 2023, **17**, 4971–4984.
- 50 Q. Su, W. Feng, D. Yang and F. Li, *Acc. Chem. Res.*, 2017, **50**, 32–40.
- 51 V. Muhr, C. Wurth, M. Kraft, M. Buchner, A. J. Baeumner, U. Resch-Genger and T. Hirsch, *Anal. Chem.*, 2017, **89**, 4868–4874.
- 52 R. Deng, J. Wang, R. Chen, W. Huang and X. Liu, *J. Am. Chem. Soc.*, 2016, **138**, 15972–15979.

